



Ultrasound-enhanced fluorescence imaging and chemotherapy of multidrug-resistant tumors using multifunctional dendrimer/carbon dot nano hybrids

Dan Li^{a,c,1}, Lizhou Lin^{b,1}, Yu Fan^{c,1}, Long Liu^b, Mingwu Shen^c, Rong Wu^b, Lianfang Du^{b,**}, Xiangyang Shi^{a,c,*}

^a Department of Interventional and Vascular Surgery, Shanghai Tenth People's Hospital, Tongji University School of Medicine, Shanghai, 200072, People's Republic of China

^b Department of Ultrasound, Shanghai General Hospital, Shanghai Jiao Tong University School of Medicine, Shanghai, 200080, People's Republic of China

^c State Key Laboratory for Modification of Chemical Fibers and Polymer Materials, College of Chemistry, Chemical Engineering and Biotechnology, Donghua University, Shanghai, 201620, People's Republic of China

ARTICLE INFO

Keywords:

Dendrimers
Carbon dots
Multidrug-resistant tumors
Ultrasound-targeted microbubble destruction technology
Fluorescence imaging
Chemotherapy

ABSTRACT

Development of innovative nanomedicine enabling enhanced theranostics of multidrug-resistant (MDR) tumors remains to be challenging. Herein, we report the development of a newly designed multifunctional yellow-fluorescent carbon dot (y-CD)/dendrimer nano hybrids as a platform for ultrasound (US)-enhanced fluorescence imaging and chemotherapy of MDR tumors. Generation 5 (G5) poly(amidoamine) dendrimers covalently modified with efflux inhibitor of D- α -tocopheryl polyethylene glycol 1000 succinate (G5-TPGS) were complexed with one-step hydrothermally synthesized y-CDs *via* electrostatic interaction. The formed G5-TPGS@y-CDs complexes were then physically loaded with anticancer drug doxorubicin (DOX) to generate (G5-TPGS@y-CDs)-DOX complexes. The developed nano hybrids display a high drug loading efficiency (40.7%), strong y-CD-induced fluorescence emission, and tumor microenvironment pH-preferred DOX release profile. Attributing to the DOX/TPGS dual drug design, the (G5-TPGS@y-CDs)-DOX complexes can overcome the multidrug resistance (MDR) of cancer cells and effectively inhibit the growth of cancer cells and tumors. Furthermore, the introduction of US-targeted microbubble destruction technology was proven to render the complexes with enhanced intracellular uptake and anticancer efficacy *in vitro* and improved chemotherapeutic efficacy and fluorescence imaging of tumors *in vivo* due to the produced sonoporation effect. The developed multifunctional dendrimer/CD nano hybrids may represent an advanced design of nanomedicine for US-enhanced theranostics of different types of MDR tumors.

1. Introduction

Breast cancer is currently the leading cause of cancer-associated mortality in women worldwide. Malignant transformation of tumors is characterized by the rapid proliferation, high invasiveness and metastasis, and multidrug resistance (MDR) of cancer cells [1,2]. Indeed, rapid development of MDR is a major obstacle in the treatment of breast cancer [3], and reversing MDR is crucial in developing therapies against this disease [4,5]. The causes of MDR are complex, however, a current study indicates that MDR is mainly related to elevated expression of P-glycoprotein (P-gp), which is a member of the adenosine triphosphate (ATP)-binding cassette (ABC) transporter family [6]. P-gp is

essentially an ATP-dependent drug pump that can pump drugs out of cells and reduce intracellular drug concentrations [7,8].

In recent years, drug efflux inhibitors have been increasingly used to overcome MDR [2]. Polyethylene glycol (PEG) 1000 vitamin E succinate (TPGS) is a P-gp inhibitor. The structure of TPGS includes a vitamin E succinate (α -TOS) and a hydroxyl ester of PEG 1000, which can inhibit the function of P-gp ATPase, disrupt mitochondrial membrane potential, and reduce intracellular ATP levels [9,10]. For these reasons, TPGS can overcome tumor MDR and increase drug accumulation within cancer cells. Furthermore, TPGS, as a mitochondriotropic substance, was reported to have mitochondrial targeting capability [11], which may accelerate the mitochondrial dysfunction [12]. Nanomaterials can

Peer review under responsibility of KeAi Communications Co., Ltd.

* Corresponding author. State Key Laboratory for Modification of Chemical Fibers and Polymer Materials, College of Chemistry, Chemical Engineering and Biotechnology, Donghua University, Shanghai, 201620, People's Republic of China.

** Corresponding author.

E-mail addresses: dulf_sh@163.com (L. Du), xshi@dhu.edu.cn (X. Shi).

¹ D. Li, L. Z. Lin, and Y. Fan contributed equally to this work.

<https://doi.org/10.1016/j.bioactmat.2020.09.015>

Received 6 August 2020; Received in revised form 6 September 2020; Accepted 17 September 2020

2452-199X/© 2020 The Authors. Publishing services by Elsevier B.V. on behalf of KeAi Communications Co., Ltd. This is an open access article under the CC BY-NC-ND license (<http://creativecommons.org/licenses/by-nc-nd/4.0/>).

be modified with TPGS to achieve the effects described above [13]. Combining TPGS with chemotherapy drugs is critical to achieve effective chemotherapy. For instance, in a previous study, we have proven that 2-dimensional nanoclays modified with TPGS and loaded with doxorubicin (DOX) are able to overcome MDR and significantly inhibit tumor growth [14]. However, the developed nanosystem just owns enhanced permeability and retention (EPR)-based passive tumor targeting and lacks simultaneous imaging guidance.

Among the numerous nano-delivery systems, carbon dots (CDs) have garnered a great deal of attention because of their low toxicity, water solubility, stability in physiologic environments, and high and tunable fluorescence emission property [15]. The unique structural characteristics of CDs have rendered their uses as a carrier to load anticancer drugs for chemotherapy. For instance, Gong et al. synthesized phosphorus- and nitrogen-doped hollow CDs for nano-delivery of DOX and fluorescence imaging [16]. Due to the lack of functionality of CDs, it is vital to combine them with other nanosystems to achieve the desired functionalities such as dual drug loading with enhanced loading efficiency and MDR overcoming.

Dendrimers, in particular, poly(amidoamine) (PAMAM) dendrimers are a class of branched, monodispersed, and synthetic macromolecules with both internal cavity and periphery functional groups [17]. The unique structural features of dendrimers allow the entrapment of inorganic nanoparticles (NPs) within their interiors and covalent conjugation of targeting ligands, drugs and bioactive ingredients for various drug delivery and imaging purposes [18–23]. It is advantageous to combine dendrimers with CDs for nanomedicinal applications. For instance, Matai et al. developed self-assembled hybrids of fluorescent CDs and PAMAM dendrimers for delivery of epirubicin and intracellular fluorescence imaging. The developed hybrids were able to induce breast cancer cell death [24], but were not applicable for suppressing multi-drug-resistant (MDR) tumors. In our previous work [25], we prepared dual drug-loaded dendrimer/CD nanohybrids (CDs-DOX)@G5-RGD-TPGS for enhanced and targeted chemotherapy and fluorescence imaging of cancer cells *in vitro* [25]. However, this system used a blue fluorescence CDs with a size of 1.4 nm that lack desired drug loading capacity, and the system was not verified in MDR cancer cells and tumor models.

Another challenge in nanomedicine involves the adequate tumor accumulation and penetration of drugs. Ultrasound (US)-targeted microbubble destruction (UTMD) technology enables the creation of numerous small holes on the surface of the cell membrane *via* a cavitation effect for enhanced delivery of exogenous macromolecules, gene transfection, and NP tumor penetration for improved tumor drug delivery [26–28]. The combination of dendrimers and UTMD technology can not only effectively enhance the delivery of genes or drugs in cells, but also achieve targeting through the ultrasonic irradiation. Previously, we have shown that under the assistance of UTMD technology, dendrimer-entrapped Au NPs coloaded with gemcitabine drug and an microRNA-21 inhibitor can be significantly delivered to tumor site for enhanced combinational therapy of a pancreatic cancer model [29]. These prior advances related to CD-based theranostic platforms, dendrimer nanotechnology, and UTMD technology prompted us to propose that a novel nanoconstruct based on CD/dendrimer nanohybrids loaded with dual drugs could be developed for US-enhanced fluorescence imaging and chemotherapy of MDR tumors *via* inhibition of the P-gp pathway.

In this present study, we report a new design of CD/dendrimer nanoconstructs for US-enhanced theranostics of MDR tumors (Scheme 1). First, yellow-fluorescent CDs (y-CDs) were synthesized *via* one-step hydrothermal treatment of 4-amino salicylic acid (4-ASA). Concurrently, generation 5 (G5) PAMAM dendrimers were covalently modified with the drug-efflux inhibitor TPGS to form G5-TPGS conjugates. After that, G5-TPGS conjugates were complexed with y-CDs *via* electrostatic interaction to form G5-TPGS@y-CDs complexes, which were then physically loaded with anticancer drug DOX to form (G5-TPGS@y-CDs)-DOX complexes. The dual drug-loaded complexes were thoroughly characterized in all physicochemical aspects. We then systematically investigated their *in vitro*

cellular uptake capacity, ability to reverse MDR, and potential for enhanced chemotherapeutic effect *in vitro* with or without UTMD. Lastly, the multifunctional CD/dendrimer nanohybrids were used for US-enhanced fluorescence imaging and chemotherapy of a xenografted human breast MDR tumor model. The main idea of this study is to develop a unique dendrimer-CD nanohybrid platform that can combine both advantages of dendrimers (easy surface modification with targeting ligands and secondary TPGS drug) and CDs (fluorescence imaging and drug loading capacity) to achieve US-boosted delivery of nanomedicine for enhanced theranostics of MDR tumors. According to our thorough literature investigation, this study represents the updated design of CD/dendrimer nanohybrids for UTMD-promoted fluorescence imaging and chemotherapy of MDR tumors *via* a P-gp inhibition pathway.

2. Experimental methods

2.1. Preparation of y-CDs

y-CDs with yellow fluorescence emission were synthesized using 4-ASA as a precursor *via* a one-step hydrothermal method [30]. In brief, 4-ASA (0.2 g) dissolved in 10 mL of water at room temperature was transferred to a 50-mL Teflon-equipped stainless steel autoclave, and heated at 180 °C for 4 h in a drying oven. After cooling down to room temperature, the y-CDs were collected by removing larger particles through centrifugation at 4000 rpm for 20 min and then the supernatant was filtrated using a 220-nm pore membrane and freeze-dried to obtain the y-CDs solid.

2.2. Preparation of G5-TPGS conjugates

TPGS (20.74 mg, dissolved in 5 mL DMSO) was mixed with 20 M equiv. of N, N'-carbonyldiimidazole (CDI, 47.25 mg, dissolved in 10 mL DMSO) under stirring for 6 h to activate the hydroxyl groups of TPGS. Then, G5 PAMAM dendrimers (17.83 mg, dissolved in 20 mL DMSO) was dropwise added to the activated TPGS solution under stirring for 72 h. The reaction mixture was dialyzed against water *via* a dialysis membrane (MWCO = 5000) and lyophilized to get the G5-TPGS product.

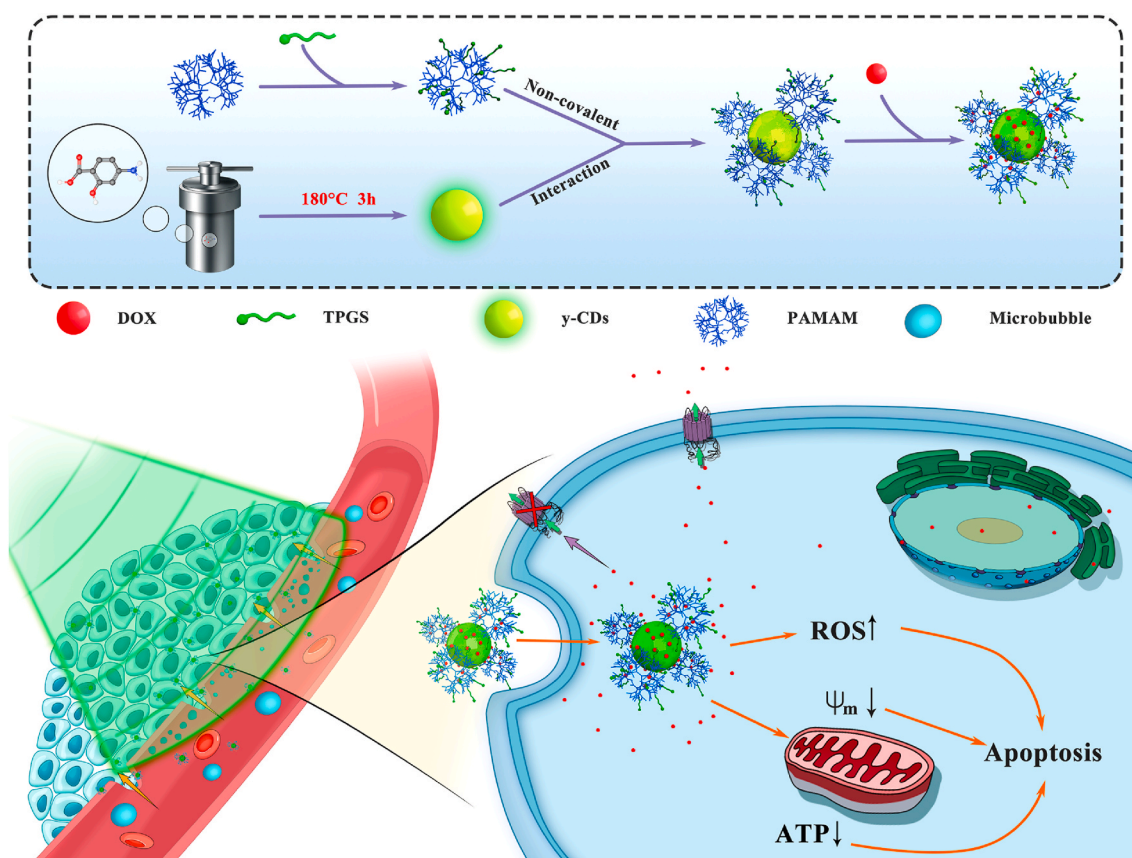
2.3. Preparation of (G5-TPGS@y-CDs)-DOX complexes

To prepare G5-TPGS@y-CDs complexes, y-CDs were mixed with G5-TPGS dendrimers to form complexes *via* either covalent interaction or non-covalent interaction at different mass ratios. For covalent interaction, the y-CDs were activated by 1-ethyl-3-(3-dimethylaminopropyl) carbodiimide hydrochloride (EDC)/N-hydroxysuccinimide in water and reacted with G5-TPGS at different G5-TPGS/y-CDs mass ratios (1:1, 3:1, 5:1 and 7:1, respectively) under magnetic stirring for 3 days. The mixture was dialyzed (MWCO of 5000) and lyophilized to get the G5-TPGS@y-CDs complexes. Alternatively, y-CDs complexes were physically mixed with G5-TPGS at a G5-TPGS/y-CDs mass ratio of 3:1 to form complexes *via* electrostatic interaction. After stirring for 24 h, the mixture was lyophilized to get the G5-TPGS@y-CDs complexes.

To load DOX within the G5-TPGS@y-CDs complexes, DOX-HCl (5.26 mg) was dissolved in methanol (600 µL) and neutralized by 10 µL of trimethylamine to form DOX. The DOX solution was then added into an aqueous solution of G5-TPGS@y-CDs (5.26 mg, 5.0 mL in water) and the mixture was vigorously stirred overnight to evaporate the methanol solvent. Then, the (G5-TPGS@y-CDs)-DOX mixture solution was centrifuged (8000 rpm) for 20 min to remove the precipitate. The supernatant solution was collected and lyophilized to obtain the (G5-TPGS@y-CDs)-DOX complexes. For comparison, single drug-loaded (G5-mPEG@y-CDs)-DOX complexes were also prepared and characterized under similar conditions.

2.4. Cell culture

Different from regular MCF-7 cells, MCF-7/ADR cells were cultured and passaged using Minimum Eagle's Medium (MEM) supplemented



Scheme 1. Schematic illustration of the formation of dual drug-loaded CD/dendrimer nano hybrids for US-enhanced theranostics of MDR tumors.

with 10% fetal bovine serum, 100 U mL⁻¹ penicillin, 100 U mL⁻¹ streptomycin, and 5 μ g/mL DOX-HCl. The drug-free γ -CDs were subjected to cytotoxicity assay, while the single-drug or dual-drug complexes were subjected to cellular uptake, fluorescence imaging, therapeutic activity, ATP level, mitochondrial membrane potential, and reactive oxygen species generation assays after the cells were incubated with them with or without UTMD.

2.5. Animal Experiments

All animal studies were approved by the Shanghai General Hospital Animal Care and Use Committee and performed in accordance with guidelines and regulations of National Ministry of Health. After intravenous injection of the dual drug-loaded CD/dendrimer nano hybrids, fluorescence imaging was performed to evaluate the EPR-based targeting to tumors with or without UTMD. In addition, we thoroughly assessed the therapeutic efficacy of the dual-drug complexes to treat the MDR tumors under UTMD through tumor volume and body weight measurements, survival rate analysis, histological hematoxylin-eosin staining (H&E) and TdT-mediated dUTP Nick-End Labeling (TUNEL) staining of tumors, and US imaging of tumor size and blood perfusion. A full description of experimental procedures can be found in the Supporting Information.

3. Results and discussion

3.1. Synthesis and characterization of γ -CDs

First, we used 4-ASA as a precursor to synthesize γ -CDs via a one-step hydrothermal method without further surface passivation or modification according to the literature [30]. The generated γ -CDs were characterized via different methods. Apparently, the γ -CDs display a characteristic absorption peak at 282 nm in the UV-vis spectrum and maximum excitation/emission wavelengths at 490 and 547 nm, respectively (Fig. 1a). The

maximum emission wavelength at 547 nm does not appear to change at different excitation wavelengths (Fig. 1b). As shown in Fig. 1c, the γ -CDs have a lifetime of 2.31 ns, and their fluorescence quantum yield was calculated to be 23.8% using quinine sulfate (in 0.1 M H₂SO₄, 56%) as a standard [31]. Fourier transform infrared (FTIR) spectroscopy was used to check the functional groups on the surface of γ -CDs (Supporting Information Fig. S1). In comparison to free 4-ASA (curve 1), γ -CDs show peaks at 3359 cm⁻¹ and 3294 cm⁻¹ (curve 2), which are related to the stretching vibration of the hydroxyl group. Meanwhile, the peaks at 1596 cm⁻¹ and 1467 cm⁻¹ correspond to the asymmetric and symmetrical stretching vibrations of the carboxyl groups, and the peak at 1258 cm⁻¹ is associated to the C–O stretching, which is consistent with the literature [30,32]. These absorption features of the γ -CDs are quite similar to those of the precursor 4-ASA, indicating that γ -CDs display abundant carboxyl and hydroxyl groups on their surface.

Transmission electron microscopy (TEM) was performed to observe the size and size distribution of γ -CDs (Fig. 1d and e). The γ -CDs display a spherical or semi-spherical shape with a mean particle size of 7.3 \pm 2.7 nm. Likewise, we show that the γ -CDs possess excellent water dispersibility and colloidal stability, and no precipitation occurs after the γ -CDs were dispersed in water for at least 3 months. Next, we also checked the fluorescence intensity of γ -CDs at 547 nm under different pHs (Supporting Information Fig. S2). It can be found that the γ -CDs exhibit the strongest fluorescence intensity at pH 6.3, and their fluorescence intensity gradually decreases with the increase and decrease of pH starting from the peak pH of 6.3. The maximum fluorescence intensity at a slightly acidic tumor microenvironmental pH ensures their tumor imaging applications with the optimum sensitivity.

3.2. Synthesis and characterization of (G5-TPGS@ γ -CDs)-DOX complexes

Next, we synthesized G5-TPGS conjugates to prepare the dual drug-loaded CD/dendrimer nano hybrids. ¹H NMR was used to characterize the

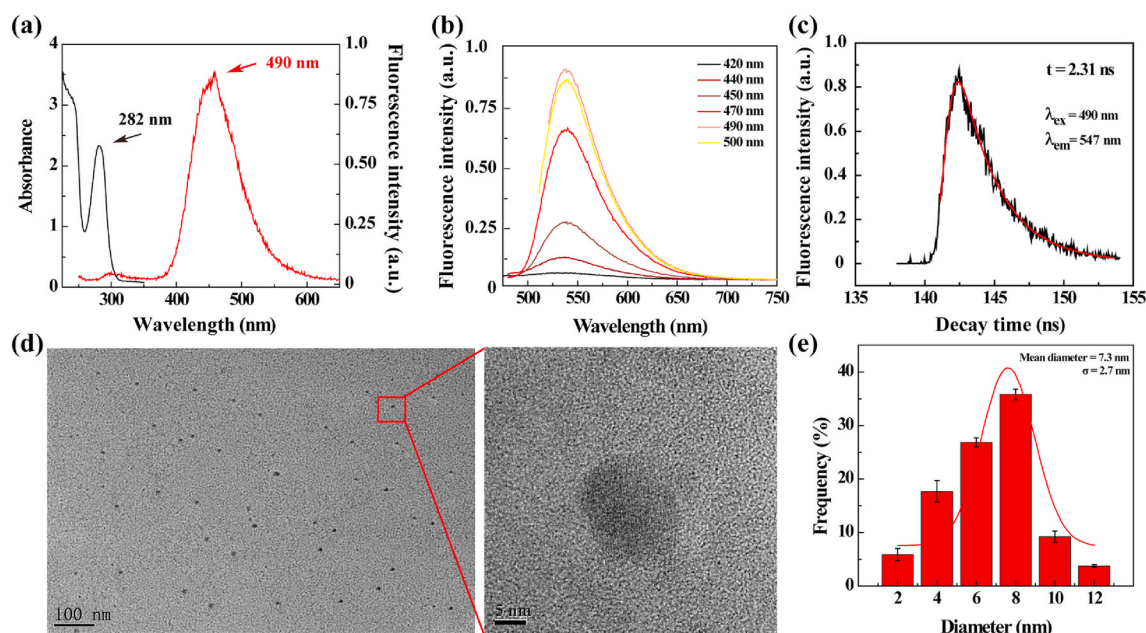


Fig. 1. (a) UV–vis spectrum (left) and fluorescence excitation spectrum (right) of y-CDs. (b) Fluorescence emission spectra of y-CDs at different excitation wavelengths. (c) Fluorescence decay curve of y-CDs ($\lambda_{\text{ex}} = 490 \text{ nm}$; $\lambda_{\text{em}} = 536 \text{ nm}$). (d) TEM image and (e) size distribution histogram of y-CDs.

TPGS and G5-TPGS conjugates (Supporting Information Fig. S3 a and b). The characteristic peaks in the range of 2.4–3.4 ppm can be assigned to the methylene protons of G5 dendrimer, and the characteristic peak at 0.7 ppm is attributed to the TPGS, in agreement with our earlier study [25]. The NMR data confirmed the successful synthesis of G5-TPGS conjugates. According to NMR integration, the number of TPGS connected to each G5 PAMAM dendrimer was estimated to be 13.4.

Next, G5-TPGS@y-CDs complexes were prepared via either EDC-mediated covalent coupling between the dendrimer leftover terminal amines and carboxyl groups of y-CDs or electrostatic interaction under different dendrimer/CD mass ratios (1:1, 3:1, 5:1, or 7:1). Fluorescence spectroscopy data reveal that y-CDs show the strongest fluorescence at the dendrimer/CD mass ratio of 3:1 for the G5-TPGS@y-CDs complexes formed via the covalent method (Supporting Information Fig. S4). Further increasing the dendrimer/CD mass ratio leads to decreased fluorescence intensity of the y-CDs, quite consistent with our previous results [25]. However, the strongest fluorescence intensity of the complexes was obtained at a dendrimer/CD mass ratio of 3:1, which is different than that reported in our earlier study. This discrepancy may have occurred because y-CDs synthesized here are much larger than the ones (1.4 nm) reported in our earlier study, and can bind more G5-TPGS conjugates on their surface. Based on this optimization, we used an electrostatic interaction to physically combine y-CDs and G5-TPGS under the dendrimer/CD mass ratio of 3:1. Apparently, compared to the covalently prepared complexes, the same complexes prepared using the non-covalent method display much higher fluorescence intensity. Hence, we decided to use the non-covalent method to prepare the G5-TPGS@y-CDs complexes at the dendrimer/CD mass ratio of 3:1 for subsequent characterization and biological applications.

UV–vis spectra of y-CDs, G5-TPGS conjugates, and G5-TPGS@y-CDs complexes dispersed in water are shown in Supporting Information Fig. S5. The G5-TPGS conjugates and y-CDs display a single featured absorption peak at 290 and 282 nm, respectively. Concurrently, the formed G5-TPGS@y-CDs complexes show a characteristic peak at 289 nm, which can be ascribed to the overlap between the absorption of G5-TPGS and y-CDs. Further, the shoulder peak at 230 nm appears in the spectra of both y-CDs and the complexes, suggesting the successful formation of the complexes. As shown in Fig. 2a, in contrast to G5-TPGS conjugates that do not show fluorescence emission, the complexes display a strong emission peak at 550 nm. The slight broader emission

peak of G5-TPGS@y-CDs than that of y-CDs may be due to the strong interaction between G5-TPGS and y-CDs [33].

Next, we physically loaded DOX within the G5-TPGS@y-CDs complexes and the dual drug-loaded (G5-TPGS@y-CDs)-DOX complexes were characterized through both UV–vis absorption and fluorescence emission spectra. We first evaluated the drug loading content (DLC) and drug loading efficiency (DLE) of the complexes to be 17.4% and 40.7%, respectively (Supporting Information Table S1). Compared with the results obtained in our previous study (DLC = 7.8% and DLE = 22.3%) [25], the DLC and DLE of the complexes are significantly improved. This may be due to the fact that compared to the previous study involved the use of dendrimer/CD mass ratio of 1:1 and smaller sized CDs (1.4 nm) to form complexes, here the DOX could be both loaded within the hydrophobic internal cavity of more G5 dendrimers [19] and loaded onto or within y-CDs with a much larger size (7.3 nm) via non-covalent hydrogen bonds [34,35] and π - π stacking [36].

As shown in Fig. 2b, as compared to the UV–vis spectra of G5-TPGS@y-CDs, the formed (G5-TPGS@y-CDs)-DOX complexes display characteristic peaks at 490 nm (DOX), 290 nm (overlapped absorptions of G5-TPGS and y-CDs), and 240 nm (DOX), indicating that DOX has been successfully loaded. The inset of Fig. 2b shows the reddish brown color of the (G5-TPGS@y-CDs)-DOX complexes in aqueous solution, which is different from the pale yellow color of the G5-TPGS@y-CDs solution, also validating the DOX loading. As compared to the fluorescence intensity of DOX-free (G5-TPGS@y-CDs) complexes and free y-CDs, the loading of DOX leads to slightly decreased fluorescence intensity of the (G5-TPGS@y-CDs)-DOX complexes (Fig. 2a), which possibly ascribed to the change of the electron charge transfer from CDs to dendrimers after DOX loading.

We also measured the surface potentials of y-CDs, G5-TPGS conjugates, G5-TPGS@y-CDs complexes, and (G5-TPGS@y-CDs)-DOX complexes to further verify the successful formation of nanohybrids (Supporting Information Table S2). The surface potential of y-CDs (-25.6 mV) increases to -5.7 mV after complexation with the positively charged G5-TPGS conjugates (15.2 mV), confirming the successful formation of G5-TPGS@y-CDs complexes via non-covalent interactions. Further loading of DOX leads to an increased surface potential of (G5-TPGS@y-CDs)-DOX complexes (6.6 mV), implying the successful DOX loading.

Meanwhile, the hydrodynamic sizes of different materials were measured to confirm the successful preparation of (G5-TPGS@y-CDs)-

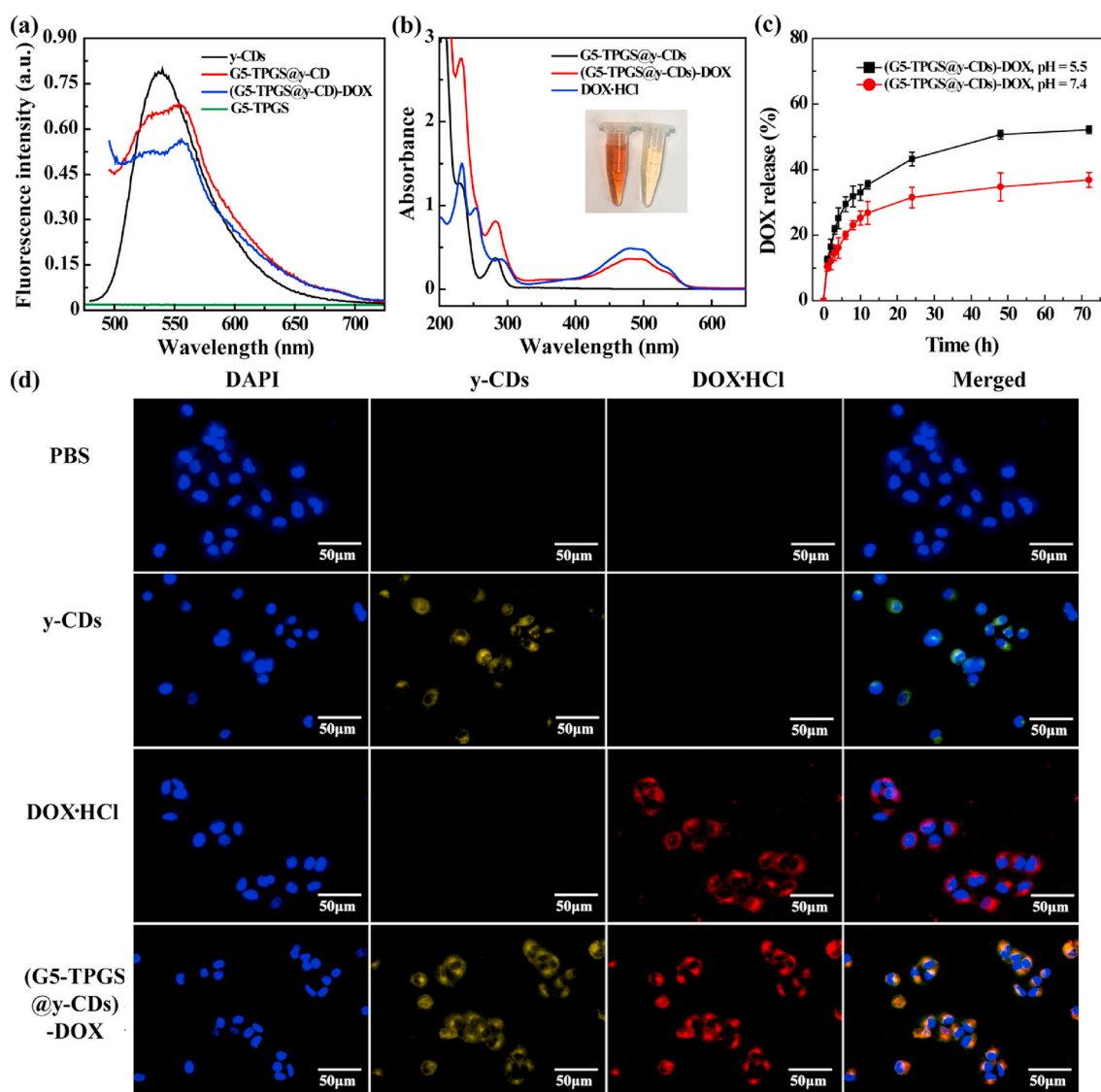


Fig. 2. (a) Fluorescence emission spectra of G5-TPGS conjugates, y-CDs, G5-TPGS@y-CDs complexes, and (G5-TPGS@y-CDs)-DOX complexes. (b) UV-vis spectra of G5-TPGS@y-CDs complexes, (G5-TPGS@y-CDs)-DOX complexes, and free DOX-HCl. Inset shows the photos of the (G5-TPGS@y-CDs)-DOX complexes (left) and G5-TPGS@y-CDs complexes (right) in aqueous solution. (c) Release kinetics of DOX from the (G5-TPGS@y-CDs)-DOX complexes at pH 5.5 and 7.4, respectively. (d) Fluorescence microscopic images of MCF-7/ADR cells incubated with free y-CDs, DOX-HCl, or (G5-TPGS@y-CDs)-DOX complexes for 6 h. Cells treated with PBS were used as control.

DOX complexes (Supporting Information Table S3). The hydrodynamic size of G5-TPGS increased from 120.8 nm to 245.1 nm after combined with y-CDs. Further loading of DOX led to a further increase of their hydrodynamic sizes to 279.2 nm, confirming the successful formation of (G5-TPGS@y-CDs)-DOX complexes. The morphology of the complexes was also observed by TEM (Fig. S6a). Clearly, the complexes display a cluster structure with a diameter around 101.8 nm. The TEM size of the complexes is different from that measured by dynamic light scattering due to the different measurement mechanisms and sample preparation processes [37]. Besides, the (G5-TPGS@y-CDs)-DOX complexes dispersed in water, PBS and MEM remained to be a stable dispersion without precipitation for at least one week (Supporting Information Fig. S6b). In addition, there was no significant change in the hydrodynamic size of (G5-TPGS@y-CDs)-DOX complexes dispersed in water for 7 days (Supporting Information Fig. S7), demonstrating the excellent stability of the complexes.

We next investigated the DOX release kinetics from the (G5-TPGS@y-CDs)-DOX complexes under different pHs (Fig. 2c). At 72 h, approximately 52% of DOX is released at pH 5.5, however, at the same time point only 36% of DOX is released at pH 7.4. This indicates that

the DOX release from the (G5-TPGS@y-CDs)-DOX complexes is pH-dependent, displaying a higher release rate under slightly acidic pH conditions than under physiological pH conditions. The rapid DOX release under slight acidic conditions may be ascribed to the protonation of DOX under acidic pH conditions, thus having improved water solubility [38]. In addition, we found that there was no appreciable effect on the release of DOX after US treatment for 2 min (Supporting Information Fig. S8) under the same conditions used for UTMD (see below). This is likely due to the fact that a single US treatment (1 MHz, 0.4 W/cm², and 2 min) is not sufficiently strong to promote DOX release from the (G5-TPGS@y-CDs)-DOX complexes.

3.3. Fluorescence imaging of MDR cancer cells *in vitro*

Due to the fluorescence emission property of the y-CDs, we first checked if the (G5-TPGS@y-CDs)-DOX complexes were able to be taken up by MDR cancer cells *in vitro* for fluorescence imaging of the cells (Fig. 2d). After 6 h incubation, compared to the PBS control, MCF-7/ADR cells (a human breast cancer adriamycin resistant cell line) treated with y-CDs and DOX-HCl display yellow-green and red fluorescence

signals, respectively, implying that both γ -CDs and DOX·HCl are able to be taken up by cells, possibly through two distinct mechanisms of phagocytosis and diffusion through cell walls [22,39]. Cells treated with the (G5-TPGS@ γ -CDs)-DOX complexes show both yellow-green and red fluorescence signals with merged images displaying orange fluorescence signal, verifying the co-localization of γ -CDs and DOX signals. This indicates that the developed (G5-TPGS@ γ -CDs)-DOX complexes are able to be internalized within the MDR cancer cells through the mechanisms described above, in good agreement with results reported in the literature [40]. The CDs together with dendrimers are able to deliver DOX in a way quite similar to DOX loaded within just dendrimer carriers without CDs [41].

To further explore the cellular uptake pathway of the complexes, MCF-7/ADR cells were first treated with endocytic pathway inhibitors of chlorpromazine (CPZ) or nystatin, followed by treatment with the (G5-TPGS@ γ -CDs)-DOX complexes (Supporting Information Fig. S9 and Fig. S10). In general, clathrin-mediated uptake pathway could be blocked by CPZ, a cationic amphiphile [42]. Apparently, the relative cellular uptake of (G5-TPGS@ γ -CDs)-DOX complexes is significantly reduced after the cells were treated with CPZ, suggesting that the internalization of complexes is related to clathrin-dependent uptake pathway. In contrast, the nystatin treatment group does not seem to result in any reduction of the cellular uptake of (G5-TPGS@ γ -CDs)-DOX complexes.

3.4. UTMD-promoted cellular uptake of complexes and anticancer activity assay

To examine whether UTMD can promote the cellular uptake of the nanohybrids, we used flow cytometry to analyze the MCF-7/ADR cells treated with the single drug-loaded (G5-*m*PEG@ γ -CDs)-DOX complexes, and (G5-TPGS@ γ -CDs)-DOX complexes without or with UTMD. We first prepared and characterized the single-drug (G5-*m*PEG@ γ -CDs)-DOX complexes. ^1H NMR was used to characterize the G5-*m*PEG conjugates (Supporting Information Fig. S3c). Through integration, the number of *m*PEG conjugated to each G5 dendrimer was estimated to be 14.7. After DOX loading, the DLC and DLE were measured to 13.72% and 58.35%, respectively (Supporting Information Table S1). At the same DOX concentration, MCF-7/ADR cells treated with the (G5-TPGS@ γ -CDs)-DOX + UTMD exhibit much stronger fluorescence than those treated with G5-*m*PEG@ γ -CDs)-DOX and (G5-TPGS@ γ -CDs)-DOX complexes ($p < 0.001$, Fig. 3a and b). This indicates that UTMD promotes the cellular uptake of the (G5-TPGS@ γ -CDs)-DOX complexes through the rendered sonoporation effect. Notably, MCF-7/ADR cells treated with the (G5-TPGS@ γ -CDs)-DOX complexes exhibit much higher fluorescence intensity than those treated with the (G5-*m*PEG@ γ -CDs)-DOX complexes at a DOX concentration of 5.0 $\mu\text{g}/\text{mL}$ ($p < 0.001$). This could be because the linked TPGS on the surface of nanohybrids can afford them with mitochondria targeting specificity, thus facilitating the enhanced cellular endocytosis of the nanohybrids [43].

To investigate the anticancer activity of the (G5-TPGS@ γ -CDs)-DOX complexes *in vitro*, we first tested the cytocompatibility of drug-free γ -CDs via a CCK-8 cell viability assay (Fig. 3c). Obviously, the viability of MCF-7 and MCF-7/ADR cells does not seem to be affected by γ -CDs at a concentration as high as 1.0 mg/mL , verifying the good cytocompatibility of γ -CDs. Next, the DOX-free G5-TPGS@ γ -CDs and G5-*m*PEG@ γ -CDs were tested to check their therapeutic activity (Supporting Information Fig. S11). In the equiv. DOX concentration range of 0.125–25 $\mu\text{g}/\text{mL}$, the DOX-free G5-*m*PEG@ γ -CDs do not seem to create any significant inhibition effect for both MCF-7 and MCF-7/ADR cells, implying their good cytocompatibility. However, the G5-TPGS@ γ -CD complexes display enhanced inhibition effect for both MCF-7 and MCF-7/ADR cells. At the complex concentration of 489.1 $\mu\text{g}/\text{mL}$, the viabilities of MCF-7 and MCF-7/ADR cells are 48% and 51%, respectively. The inhibitory effect of DOX-free complexes is likely due to the linked α -TOS, the active component of TPGS that can inhibit the growth of cancer cells without the necessity to be released [37,44]. It is noticeable

that the concentrations of G5-TPGS@ γ -CDs complexes used are equivalent to those of DOX for the DOX-loaded complexes (*vide infra*), allowing for reasonable comparison of the activity of single drug-versus dual drug-loaded complexes.

MCF-7/ADR cells display much higher levels of P-gp on the cell surface than regular MCF-7 cells [45]. Hence, substrates of P-gp (such as DOX) can be transported extracellularly, causing MDR of cancer cells [46]. Here, we first assessed the ability of (G5-TPGS@ γ -CDs)-DOX complexes to inhibit both MCF-7 and MCF-7/ADR cells in the absence and presence of UTMD. For regular MCF-7 cells, at the DOX concentration of 0.25 $\mu\text{g}/\text{mL}$ or above, the inhibitory effect follows the order of free DOX·HCl > (G5-TPGS@ γ -CDs)-DOX + UTMD > (G5-TPGS@ γ -CDs)-DOX > (G5-*m*PEG@ γ -CDs)-DOX (Fig. 3d). At a DOX concentration of 25 $\mu\text{g}/\text{mL}$, the cell viabilities of the respective groups are 8.6%, 12.5%, 21.5%, and 42.9%, respectively. These results indicate that dual drug-loaded (G5-TPGS@ γ -CDs)-DOX complexes have a better inhibitory effect than the single DOX-loaded (G5-*m*PEG@ γ -CDs)-DOX complexes and single TPGS-loaded G5-TPGS@ γ -CDs complexes (e.g., cell viability of 48% at equiv. DOX concentration of 25 $\mu\text{g}/\text{mL}$). The TPGS may play two roles in the enhancement effect: (1) increasing the accumulation of DOX within MCF-7 cells through mitochondrial targeting, and (2) exerting the α -TOS cancer cell inhibitory effect. With the assistance of UTMD, the inhibitory effect of (G5-TPGS@ γ -CDs)-DOX complexes can be further enhanced through the generated sonoporation effect.

Next, we verified the inhibitory effect of MCF-7/ADR cells treated with the (G5-TPGS@ γ -CDs)-DOX complexes (Fig. 3e). Similar to the case of regular MCF-7 cell treatment, the MCF-7/ADR cells display decreased viability with the increase of DOX concentration for all formulations. It is obvious that the inhibition effect of both free DOX·HCl and (G5-*m*PEG@ γ -CDs)-DOX complexes is quite limited when compared to that of the (G5-TPGS@ γ -CDs)-DOX complexes, which are able to reduce the cell viability to 27.8% at a DOX concentration of 25 $\mu\text{g}/\text{mL}$. Without the conjugation of TPGS, the P-gp-induced MDR effect cannot be overcome by free DOX·HCl and (G5-*m*PEG@ γ -CDs)-DOX complexes. Instead, the developed dual drug-loaded (G5-TPGS@ γ -CDs)-DOX complexes should be able to overcome the MDR effect [47]. Specifically, TPGS can inhibit the activity of P-gp ATPase to lead to intracellular accumulation of DOX, bind to mitochondrial respiratory complexes to cause mitochondrial dysfunction, and induce cellular apoptosis [48]. In the presence of UTMD, the cell viability can be further decreased to 16.8% after treatment with the dual-drug complexes. Apparently, the adoption of UTMD enables significantly enhanced cancer cell inhibitory effect ($p < 0.01$), similar to the treatment of regular MCF-7 cells using the dual-drug complexes. The *in vitro* therapeutic activity of different DOX-associated formulations was further quantitatively characterized by their half-maximal inhibitory concentrations (IC_{50} s) after both MCF-7 and MCF-7/ADR cells were treated for 24 h (Supporting Information Table S4). For regular MCF-7 cells, the IC_{50} of the dual-drug complexes is 4.6 times lower than the single-drug complexes, and UTMD could render the IC_{50} of the dual-drug complexes with 2.9 times lower than without UTMD. Similarly, for the MDR MCF-7/ADR cells, the TPGS/DOX dual-drug complexes have a more than 2.8 and 3.2 times lower IC_{50} than the single DOX complexes and free DOX·HCl, respectively, and the application of UTMD can further decrease the IC_{50} of dual-drug complexes around 1.8 times lower than without UTMD.

3.5. Mechanistic evaluation of MDR reversal of cancer cells

To confirm the TPGS-induced MDR reversal of cancer cells, we next investigated the mitochondrial membrane potential, ATP level, and reactive oxygen species (ROS) generation after the MDR cells were treated with dual-drug complexes since these parameters are cooperative to prove the effective treatment. As a P-gp inhibitor, TPGS can bind to mitochondria and induce decreased membrane potential, thus reducing the level of intracellular ATP, increasing ROS levels and activating cell apoptosis to overcome MDR [12]. The mitochondrial dysfunction was

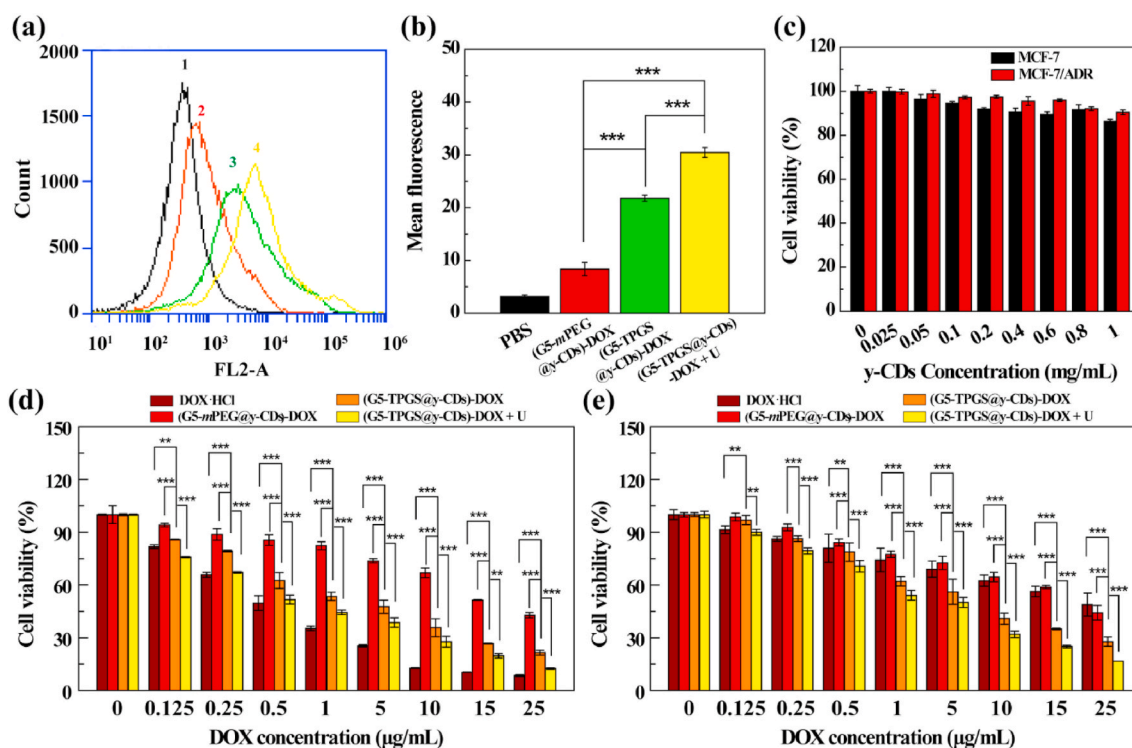


Fig. 3. (a) Fluorescence histogram and (b) mean fluorescence of cells after treatment with PBS (1), (G5-mPEG@y-CDs)-DOX complexes (2), (G5-TPGS@y-CDs)-DOX complexes (3), and (G5-TPGS@y-CDs)-DOX + UTMD (4) for 6 h at a DOX concentration of 5.0 $\mu\text{g/mL}$. (c) Viability of MCF-7 and MCF-7/ADR cells treated with y-CDs at different concentrations for 24 h. Viability of (d) MCF-7 and (e) MCF-7/ADR cells treated with free DOX-HCl, (G5-mPEG@y-CDs)-DOX complexes, (G5-TPGS@y-CDs)-DOX complexes, and (G5-TPGS@y-CDs)-DOX + UTMD (for short, + U) at different DOX concentrations for 24 h.

quantified by measuring its membrane potential using a detection kit (JC-1). JC-1 is a fluorescence probe that detects alterations of mitochondrial membrane potential, and emits red fluorescence at a high membrane potential and green fluorescence at a low potential [14]. We used the red/green fluorescence intensity ratio of JC-1 to quantify the intracellular mitochondrial membrane potential (Fig. 4a). At the same DOX concentration, the red/green fluorescence ratio in cells treated with dual-drug (G5-TPGS@y-CDs)-DOX complexes is significantly lower than that treated with the single-drug (G5-mPEG@y-CDs)-DOX complexes ($p < 0.001$ at DOX concentration of 5 $\mu\text{g/mL}$ or above, Supporting Information Fig. S12). This finding demonstrates that the loaded TPGS induces decreased mitochondrial membrane potential.

As mentioned above, the process of drug (e.g., DOX) to be extruded out of cells *via* P-gp is ATP-dependent. The intracellular ATP levels in MCF-7/ADR cells after incubation with single-drug (G5-mPEG@y-CDs)-DOX or dual-drug (G5-TPGS@y-CDs)-DOX complexes for 6, 12, and 24 h were compared (Fig. 4b). It is apparent that the intracellular ATP in the dual-drug group is much lower than that in the single-drug group at the same treatment time period ($p < 0.05$). Particularly, at 24 h treatment, the ATP levels are 36.6% and 67.2%, respectively for the (G5-TPGS@y-CDs)-DOX and (G5-mPEG@y-CDs)-DOX groups. The lower intracellular ATP level is beneficial to inhibit the activity of P-gp pumps on cell membranes to reverse MDR.

Both TPGS and DOX promote generation of ROS in cancer cells, resulting in cell apoptosis [49,50]. We then evaluated the ROS levels in MCF-7/ADR cells treated with (G5-TPGS@y-CDs)-DOX, (G5-mPEG@y-CDs)-DOX, and G5-TPGS@y-CDs complexes for 6 h through flow cytometry (Fig. 4c). 2, 7-Dichlorofluorescein diacetate (DCFH-DA) can be oxidized to generate DCF in the presence of ROS to emit green fluorescence, thus can be used as an ROS probe [51]. MCF-7/ADR cells treated with the dual-drug (G5-TPGS@y-CDs)-DOX complexes display significantly stronger fluorescence intensity than those treated with the single-drug (G5-mPEG@y-CDs)-DOX and G5-TPGS@y-CDs complexes at the same DOX or equiv. DOX concentrations ($p < 0.001$). It also appears that single-drug (G5-mPEG@y-CDs)-DOX complexes are more

effective than G5-TPGS@y-CDs complexes to generate ROS under the same DOX or equiv. DOX concentrations ($p < 0.001$). Taken together with the ATP level and mitochondria membrane potential measurements, our results collectively validate the effective reversal and treatment of MDR cancer cells using the designed dual-drug complexes.

3.6. *In vivo* fluorescence imaging

With the fluorescence properties rendered by y-CDs, we next checked the ability of the dual-drug (G5-TPGS@y-CDs)-DOX complexes for tumor fluorescence imaging in the presence and absence of UTMD. Nude mice bearing MCF-7/ADR xenografts were imaged *in vivo* after intravenous injection of y-CDs and (G5-TPGS@y-CDs)-DOX complexes (with or without UTMD). As presented in Supporting Information Figs. S13a–b, upon injection of the (G5-TPGS@y-CDs)-DOX complexes, the fluorescence signal could be viewed in the tumor region even at 6 h post-injection, which may be due to the EPR-based passive tumor targeting effect since the nanohybrids have a relative large size of 101.8 nm. In contrast, the fluorescence signal of tumors in the y-CDs group was significantly weaker than those in the other groups at the same time points, suggesting that the free y-CDs could be quickly metabolized due to their small size (7.3 nm). Furthermore, with the assistance of UTMD, a significantly enhanced fluorescence signal was observed stably in the tumor region, validating the role played by the UTMD-rendered sonoporation effect.

The UTMD-rendered enhanced tumor fluorescence imaging was further demonstrated by *ex vivo* organ and tumor fluorescence imaging at 6 h post-injection, where the strongest *ex vivo* tumor fluorescence signal was observed in the (G5-TPGS@y-CDs)-DOX + U group (Supporting Information Fig. S14). As recorded in Supporting Information Fig. S15, the fluorescence intensities of different organs in the (G5-TPGS@y-CDs)-DOX and (G5-TPGS@y-CDs)-DOX + U group follow the order of liver > kidney > lung > spleen > heart. In addition, the fluorescence intensities of different organs and tumor in the y-CDs group follow the order of liver > kidney > spleen > lung > tumor > heart.

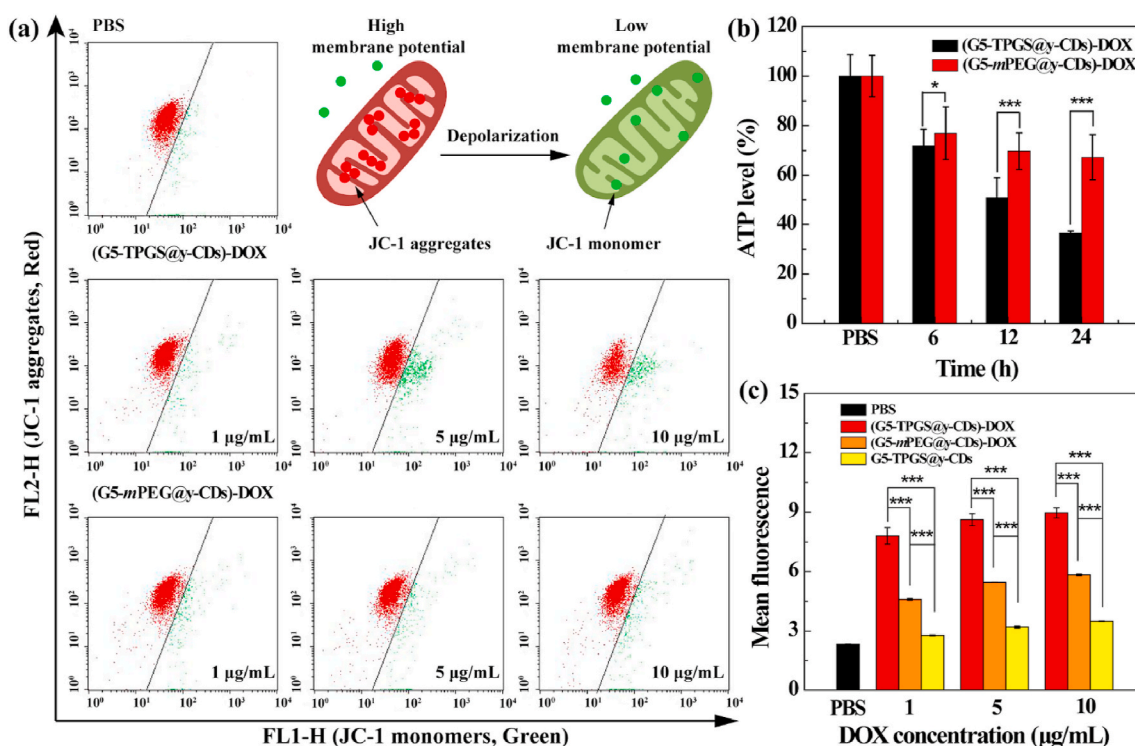


Fig. 4. (a) Flow cytometry analysis results of mitochondrial membrane potential in MCF-7/ADR cells after incubation with (G5-*mPEG@y-CDs*)-DOX and (G5-TPGS@*y-CDs*)-DOX complexes. (b) Intracellular ATP levels in MCF-7/ADR cells after incubation with (G5-*mPEG@y-CDs*)-DOX and (G5-TPGS@*y-CDs*)-DOX complexes for 6, 12, and 24 h, respectively. (c) Flow cytometry assay of the 2, 7-dichlorofluorescein (DCF) fluorescence within MCF-7/ADR cells to reflect the levels of ROS after 6 h treatment with the (G5-TPGS@*y-CDs*)-DOX, (G5-*mPEG@y-CDs*)-DOX and G5-TPGS@*y-CDs* complexes, respectively.

3.7. Therapeutic efficacy of MDR tumors *in vivo*

We lastly checked the therapeutic efficacy of the dual-drug complexes to treat xenografted MCF-7/ADR tumor model *in vivo* (Fig. 5a). As shown in Fig. 5b, the tumor inhibitory effect after 20 days' treatment follows the order of (G5-TPGS@*y-CDs*)-DOX + UTMD > (G5-TPGS@*y-CDs*)-DOX > (G5-*mPEG@y-CDs*)-DOX > free DOX·HCl > saline. Notably, we have demonstrated that single UTMD treatment has no obvious inhibition effect on the tumor growth [28]. The significantly enhanced tumor inhibition ability of the (G5-TPGS@*y-CDs*)-DOX + UTMD treatment is attributed to the TPGS-based dual drug design to effectively reverse MDR in tumors and enhance the antitumor activity, and the applied UTMD technique to promote tumor accumulation of the complexes. The body weights of mice treated with the (G5-TPGS@*y-CDs*)-DOX with or without UTMD do not change significantly when compared with those treated with the (G5-*mPEG@y-CDs*)-DOX complexes and free DOX·HCl (Fig. 5c), indicating that all treatments do not seem to generate systemic toxicity of mice. Interestingly, different from free DOX treatment of regular tumor types to induce significant side effects [52], free DOX does not exhibit toxicity in MDR tumor mice. Furthermore, the mouse survival rate after the whole experimental time period shows that the (G5-TPGS@*y-CDs*)-DOX + UTMD and (G5-TPGS@*y-CDs*)-DOX groups have much higher survival rates than the (G5-*mPEG@y-CDs*)-DOX and free DOX·HCl groups, and all mice are dead in the saline control group (Fig. 5d). These results further confirm that the treatment with (G5-TPGS@*y-CDs*)-DOX + UTMD is the most effective for MDR tumor chemotherapy.

To check the tumor treatment efficacy, ultrasound imaging was used to monitor the tumor size and blood perfusion (Fig. 5e). As shown in the B-mode images, the tumor sizes in groups display an order of (G5-TPGS@*y-CDs*)-DOX + UTMD < (G5-TPGS@*y-CDs*)-DOX < (G5-*mPEG@y-CDs*)-DOX < free DOX·HCl < saline. The treatment of (G5-TPGS@*y-CDs*)-DOX + UTMD appears to be more effective than that of (G5-TPGS@*y-CDs*)-DOX to reduce tumor volume. This clearly indicates the UTMD-played enhancing role for chemotherapy of MDR tumors. Since contrast-

enhanced ultrasound (CEUS) imaging is a reliable modality to reveal vascular flow within tumors and to evaluate tumor treatment effect [53,54], subcutaneous tumor vascularity was also evaluated post-treatment using CEUS imaging to assess the therapeutic effects. Clearly, the most significant intratumoral blood perfusion can be detected in the (G5-TPGS@*y-CDs*)-DOX + UTMD group, indicating the best chemotherapeutic effect and prognosis. As expected, increased blood perfusion results in the enhanced drug permeability and hence enhanced tumor chemotherapeutic effect.

Next, we evaluated the therapeutic efficacy of different groups through hematoxylin and eosin (H&E) and TdT-mediated dUTP Nick-End Labeling (TUNEL) staining of tumor slices (Supporting Information Fig. S16). Apparently, in the saline and free DOX·HCl groups, the tumor shows well-shaped cell morphology and no obvious necrotic and apoptotic areas emerging in the tumor site. For the free DOX·HCl group, this may have occurred for the MDR tumor model that is resistant to DOX treatment. A small necrotic and apoptotic areas in the tumor site emerge for the single-drug (G5-*mPEG@y-CDs*)-DOX group, while (G5-TPGS@*y-CDs*)-DOX and (G5-TPGS@*y-CDs*)-DOX + UTMD groups display much larger necrotic and apoptotic areas, demonstrating that the dual-drug (G5-TPGS@*y-CDs*)-DOX complexes are able to inhibit the MDR tumors and the enhanced treatment effect can be rendered by UTMD. Quantitative analysis of the tumor cell apoptosis rate (Supporting Information Fig. S17) shows the ordering of the treatment efficacy as (G5-TPGS@*y-CDs*)-DOX + UTMD group (79.2%) > (G5-TPGS@*y-CDs*)-DOX group (59.0%) > (G5-*mPEG@y-CDs*)-DOX group (23.0%) > free DOX·HCl group (7.3%) > saline group (4.4%).

Lastly, H&E staining was also used to examine the morphological changes in the organs of mice after different treatments (Supporting Information Fig. S18). Obviously, all the treatment groups do not seem to generate any significant changes in the morphology of major organs when compared to the saline control group. Overall, our results indicate that the treatment of dual drug (G5-TPGS@*y-CDs*)-DOX complexes with or without UTMD does not generate organ compatibility issues and displays a quite low systemic toxicity.

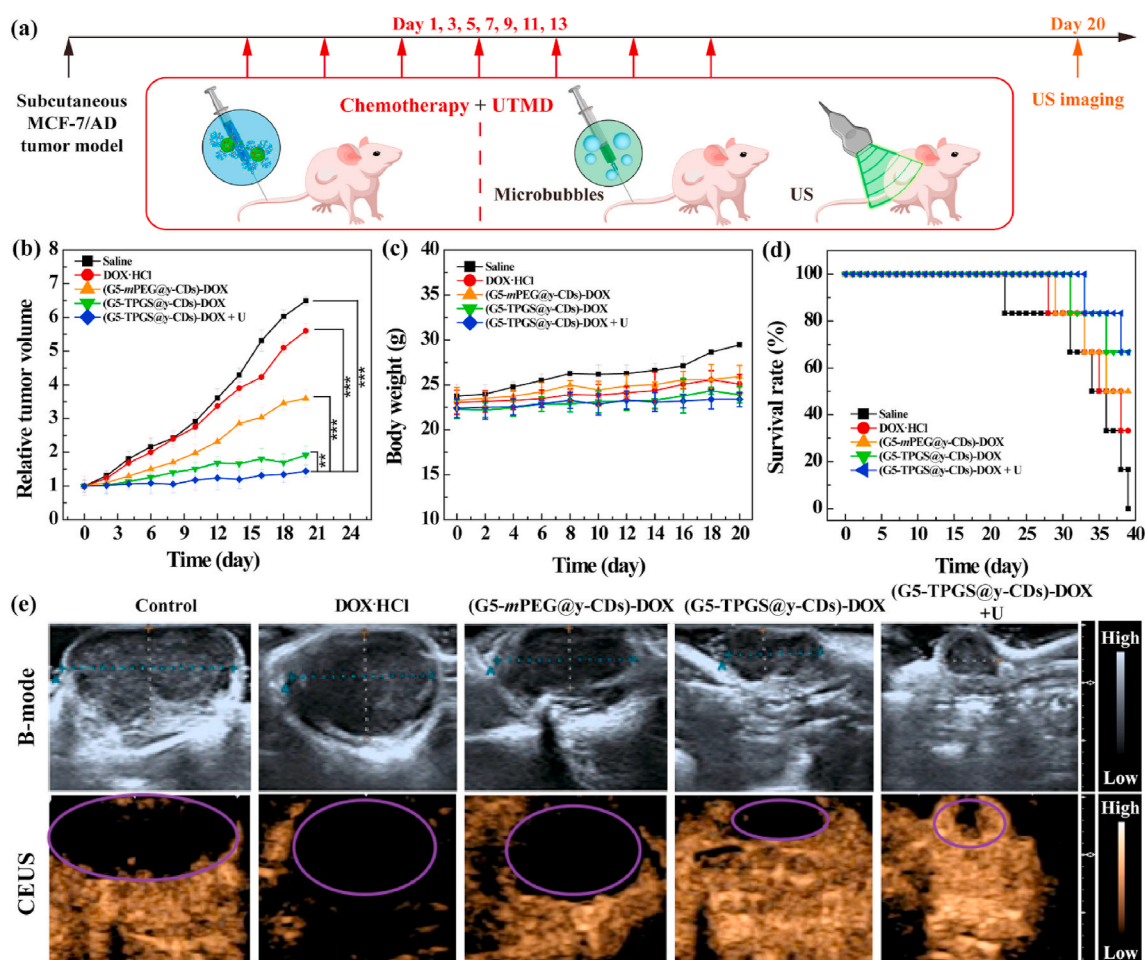


Fig. 5. (a) The therapeutic schedule of (G5-TPGS@y-CDs)-DOX + UTMD treatment *in vivo*. (b) Relative tumor volumes after tumor-bearing mice were intravenously injected with saline (100 μ L), free DOX-HCl (5 mg/kg, 100 μ L), (G5-mPEG@y-CDs)-DOX ([DOX] = 5 mg/kg, 100 μ L), (G5-TPGS@y-CDs)-DOX ([DOX] = 5 mg/kg, 100 μ L), or (G5-TPGS@y-CDs)-DOX + UTMD ([DOX] = 5 mg/kg, 100 μ L) per mouse for 20 days (one injection per 2 days for 20 days). (c) Body weights of mice as function of time post-injection after undergoing different treatments. (d) Survival rate of tumor-bearing mice versus time post-injection after different treatments. (e) B-mode ultrasound and CEUS images of tumor-bearing mice *in vivo*. Dotted lines and ellipses/circles indicate the tumor regions.

4. Conclusion

In summary, we developed a multifunctional nanomedicine based on y-CD/dendrimer nanohybrids loaded with dual drugs of TPGS and DOX for US-enhanced fluorescence imaging and chemotherapy of MDR tumors. We show that through electrostatic interaction, G5-TPGS conjugates and y-CDs can be complexed for further DOX loading with a high drug loading capacity, and the formed dual-drug complexes display tumor micro-environmental pH-preferred DOX release. With the loaded TPGS, an inhibitor of P-gp, the dual-drug complexes are able to overcome the MDR of cancer cells through reducing the intracellular ATP level and mitochondria membrane potential and enhancing the ROS generation, thus significantly inhibiting the MDR cancer cells. Additionally, the application of UTMD further enhances the chemotherapeutic efficacy of the dual drug (G5-TPGS@y-CDs)-DOX complexes to treat cancer cells and a subcutaneous tumor model with MDR through the produced sonoporation effect. This can also be reflected through the enhanced tumor fluorescence imaging and be characterized to display enhanced intratumoral blood perfusion for the *in vivo* tumor therapy. With the versatile dendrimer nanotechnology, the developed CD/dendrimer nanohybrid platform may also be modified with targeting ligands to achieve specific targeting of a particular cancer type for improved cancer theranostics. Overall, the developed tumor MDR-overcoming nanomedicine with fluorescence imaging ability represents a new design through combination of CDs and dendrimers, and may be employed for US-enhanced theranostics of other tumor types.

CRediT authorship contribution statement

Dan Li: Methodology, Formal analysis, Investigation, Writing - original draft. **Lizhou Lin:** Methodology, Formal analysis, Investigation. **Yu Fan:** Formal analysis, Visualization, Writing - review & editing. **Long Liu:** Methodology, Resources. **Mingwu Shen:** Supervision, Funding acquisition. **Rong Wu:** Resources, Supervision. **Lianfang Du:** Resources, Supervision, Project administration. **Xiangyang Shi:** Conceptualization, Writing - review & editing, Supervision, Project administration, Funding acquisition.

Conflicts of interest

There are no conflicts of interest to declare.

Acknowledgements

This research has been financially supported by the Science and Technology Commission of Shanghai Municipality (20520710300, 19XD1400100, 19YF1440400 and 19410740200), the National Key R&D Program (2017YFE0196200), and the National Natural Science Foundation of China (81761148028 and 21773026).

Appendix A. Supplementary data

Supplementary data to this article can be found online at <https://doi.org/10.1016/j.bioactmat.2020.09.015>.

References

- [1] A.M. Chen, M. Zhang, D. Wei, D. Stueber, O. Taratula, T. Minko, H. He, Co-delivery of doxorubicin and bcl-2 siRNA by mesoporous silica nanoparticles enhances the efficacy of chemotherapy in multidrug-resistant cancer cells, *Small* 5 (23) (2009) 2673–2677.
- [2] A. Palmeira, E. Sousa, M.H. Vasconcelos, M.M. Pinto, Three decades of P-gp inhibitors: skimming through several generations and scaffolds, *Curr. Med. Chem.* 19 (13) (2012) 1946–2025.
- [3] L.A. Doyle, W.D. Yang, L.V. Abruzzo, T. Krogmann, Y.M. Gao, A.K. Rishi, D.D. Ross, A multidrug resistance transporter from human MCF-7 breast cancer cells, *Proc. Natl. Acad. Sci. U.S.A.* 95 (26) (1998) 15665–15670.
- [4] X. Wei, Y. Wang, X. Xiong, X. Guo, L. Zhang, X.B. Zhang, S.B. Zhou, Codelivery of a pi-pi stacked dual anticancer drug combination with nanocarriers for overcoming multidrug resistance and tumor metastasis, *Adv. Funct. Mater.* 26 (45) (2016) 8266–8280.
- [5] X. Guo, X. Wei, Y.T. Jing, S.B. Zhou, Size changeable nanocarriers with nuclear targeting for effectively overcoming multidrug resistance in cancer therapy, *Adv. Mater.* 27 (41) (2015) 6450–6456.
- [6] M.M. Gottesman, T. Fojo, S.E. Bates, Multidrug resistance in cancer: role of ATP-dependent transporters, *Nat. Rev. Cancer* 2 (1) (2002) 48–58.
- [7] S.G. Aller, J. Yu, A. Ward, Y. Wang, S. Chittaboina, R. Zhuo, P.M. Harrell, Y.T. Trinh, Q. Zhang, I.L. Urbatsch, G. Chang, Structure of P-glycoprotein reveals a molecular basis for poly-specific drug binding, *Science* 323 (5922) (2009) 1718–1722.
- [8] X. Wei, L. Liu, X. Guo, Y. Wang, J. Zhao, S. Zhou, Light-activated ROS-responsive nanoplateform codelivering apatinib and doxorubicin for enhanced chemo-photodynamic therapy of multidrug-resistant tumors, *ACS Appl. Mater. Interfaces* 10 (21) (2018) 17672–17684.
- [9] J.M. Dintaman, J.A. Silverman, Inhibition of P-glycoprotein by D-alpha-tocopheryl polyethylene glycol 1000 succinate (TPGS), *Pharm. Res. (N. Y.)* 16 (10) (1999) 1550–1556.
- [10] Y.-X. Zhu, H.-R. Jia, G. Gao, G.-Y. Pan, Y.-W. Jiang, P. Li, N. Zhou, C. Li, C. She, N.W. Ulrich, Z. Chen, F.-G. Wu, Mitochondria-acting nanomicelles for destruction of cancer cells via excessive mitophagy/autophagy-driven lethal energy depletion and phototherapy, *Biomaterials* 232 (2020) 119668.
- [11] A.G. Assanhou, W. Li, L. Zhang, L. Xue, L. Kong, H. Sun, R. Mo, C. Zhang, Reversal of multidrug resistance by co-delivery of paclitaxel and lonidamine using a TPGS and hyaluronic acid dual-functionalized liposome for cancer treatment, *Biomaterials* 73 (2015) 284–295.
- [12] C. Yang, T. Wu, Y. Qi, Z. Zhang, Recent advances in the application of vitamin E TPGS for drug delivery, *Theranostics* 8 (2) (2018) 464–485.
- [13] R.G. Tuguntaev, S. Chen, A.S. Eltahan, A. Mozhi, S. Jin, J. Zhang, C. Li, P.C. Wang, X.-J. Liang, P-gp inhibition and mitochondrial impairment by dual-functional nanostructure based on vitamin E derivatives to overcome multidrug resistance, *ACS Appl. Mater. Interfaces* 9 (20) (2017) 16901–16913.
- [14] T. Jiang, C. Zhang, W. Sun, X. Cao, G. Choi, J.-H. Choy, X. Shi, R. Guo, Doxorubicin encapsulated in TPGS-modified 2D-nanodisks overcomes multidrug resistance, *Chem. Eur. J.* 26 (2020) 2470–2477.
- [15] K. Hala, Y. Zhang, Y. Wang, E.P. Giannelis, R. Zboril, A.L. Rogach, Carbon dots-Emerging light emitters for bioimaging, cancer therapy and optoelectronics, *Nano Today* 9 (5) (2014) 590–603.
- [16] X. Gong, Q. Zhang, Y. Gao, S. Shuang, M.M.F. Choi, C. Dong, Phosphorus and nitrogen dual-doped hollow carbon dot as a nanocarrier for doxorubicin delivery and biological imaging, *ACS Appl. Mater. Interfaces* 8 (18) (2016) 11288–11297.
- [17] Y. Fan, W. Sun, X. Shi, Design and biomedical applications of poly(amidoamine)-dendrimer-based hybrid nanoarchitectures, *Small Methods* 1 (12) (2017) 1700224.
- [18] J.Y. Zhu, X.Y. Shi, Dendrimer-based nanodevices for targeted drug delivery applications, *J. Mater. Chem. B* 1 (34) (2013) 4199–4211.
- [19] F. Fu, Y. Wu, J. Zhu, S. Wen, M. Shen, X. Shi, Multifunctional lactobionic acid-modified dendrimers for targeted drug delivery to liver cancer cells: investigating the role played by PEG spacer, *ACS Appl. Mater. Interfaces* 6 (18) (2014) 16416–16425.
- [20] L. Kong, Y. Wu, C.S. Alves, X. Shi, Efficient delivery of therapeutic siRNA into glioblastoma cells using multifunctional dendrimer-entrapped gold nanoparticles, *Nanomedicine* 11 (23) (2016) 3103–3115.
- [21] Z. Xiong, M. Shen, X. Shi, Dendrimer-based strategies for cancer therapy: recent advances and future perspectives, *Sci. China Mater.* 61 (11) (2018) 1387–1403.
- [22] Y. Fan, J.L. Zhang, M.H. Shi, D. Li, C.H. Lu, X.Y. Cao, C. Peng, S.G. Mignani, J.P. Majoral, X.Y. Shi, Poly(amidoamine) dendrimer-coordinated copper(ii) complexes as a theranostic nanoplateform for the radiotherapy-enhanced magnetic resonance imaging and chemotherapy of tumors and tumor metastasis, *Nano Lett.* 19 (2) (2019) 1216–1226.
- [23] Y. Fan, W.Z. Tu, M.W. Shen, X.M. Chen, Y.S. Ning, J.J. Li, T.F. Chen, H. Wang, F.F. Yin, Y. Liu, X.Y. Shi, Targeted tumor hypoxia dual-mode CT/MR imaging and enhanced radiation therapy using dendrimer-based nanosensitizers, *Adv. Funct. Mater.* 30 (13) (2020) 1909285.
- [24] I. Matai, A. Sachdev, P. Gopinath, Self-assembled hybrids of fluorescent carbon dots and PAMAM dendrimers for epirubicin delivery and intracellular imaging, *ACS Appl. Mater. Interfaces* 7 (21) (2015) 11423–11435.
- [25] D. Li, Y. Fan, M. Shen, I. Banyai, X. Shi, Design of dual drug-loaded dendrimer/carbon dot nanohybrids for fluorescence imaging and enhanced chemotherapy of cancer cells, *J. Mater. Chem. B* 7 (2) (2019) 277–285.
- [26] B. Zeqiri, M. Hodnett, A.J. Carroll, Studies of a novel sensor for assessing the spatial distribution of cavitation activity within ultrasonic cleaning vessels, *Ultrasonics* 44 (1) (2006) 73–82.
- [27] F. Nie, H.-X. Xu, M.-D. Lu, Y. Wang, Q. Tang, Anti-angiogenic gene therapy for hepatocellular carcinoma mediated by microbubble-enhanced ultrasound exposure: an in vivo experimental study, *J. Drug Target.* 16 (5) (2008) 389–395.
- [28] L. Xing, Q. Shi, K. Zheng, M. Shen, J. Ma, F. Li, Y. Liu, L. Lin, W. Tu, Y. Duan, L. Du, Ultrasound-mediated microbubble destruction (UMMD) facilitates the delivery of CA19-9 targeted and paclitaxel loaded mPEG-PLGA-PLL nanoparticles in pancreatic cancer, *Theranostics* 6 (10) (2016) 1573–1587.
- [29] L. Lin, Y. Fan, F. Gao, L. Jin, D. Li, W. Sun, F. Li, P. Qin, Q. Shi, X. Shi, L. Du, UTMD-promoted Co-delivery of gemcitabine and miR-21 inhibitor by dendrimer-entrapped gold nanoparticles for pancreatic cancer therapy, *Theranostics* 8 (7) (2018) 1923–1939.
- [30] L. Shi, L. Li, X. Li, G. Zhang, Y. Zhang, C. Dong, S. Shuang, Excitation-independent yellow-fluorescent nitrogen-doped carbon nanodots for biological imaging and paper-based sensing, *Sens. Actuators, B* 251 (2017) 234–241.
- [31] X.Y. Xu, R. Ray, Y.L. Gu, H.J. Ploehn, L. Gearheart, K. Raker, W.A. Scrivens, Electrophoretic analysis and purification of fluorescent single-walled carbon nanotube fragments, *J. Am. Chem. Soc.* 126 (40) (2004) 12736–12737.
- [32] M. Zheng, S. Ruan, S. Liu, T. Sun, D. Qu, H. Zhao, Z. Xie, H. Gao, X. Jing, Z. Sun, Self-targeting fluorescent carbon dots for diagnosis of brain cancer cells, *ACS Nano* 9 (11) (2015) 11455–11461.
- [33] G. Tong, J. Wang, R. Wang, X. Guo, L. He, F. Qiu, G. Wang, B. Zhu, X. Zhu, T. Liu, Amorphous carbon dots with high two-photon fluorescence for cellular imaging passivated by hyperbranched poly(amino amine), *J. Mater. Chem. B* 3 (4) (2015) 700–706.
- [34] Q. Zeng, D. Shao, X. He, Z. Ren, W. Ji, C. Shan, S. Qu, J. Li, L. Chen, Q. Li, Carbon dots as a trackable drug delivery carrier for localized cancer therapy in vivo, *J. Mater. Chem. B* 4 (30) (2016) 5119–5126.
- [35] B. Wang, S. Wang, Y. Wang, Y. Lv, H. Wu, X. Ma, M. Tan, Highly fluorescent carbon dots for visible sensing of doxorubicin release based on efficient nanosurface energy transfer, *Biotechnol. Lett.* 38 (1) (2016) 191–201.
- [36] E. Aznar, R. Casasus, B. Garcia-Acosta, M.D. Marcos, R. Martinez-Manez, Photochemical and chemical two-channel control of functional nanogated hybrid architectures, *Adv. Mater.* 19 (17) (2007) 2228–2231.
- [37] J.Y. Zhu, L.F. Zheng, S.H. Wen, Y.Q. Tang, M.W. Shen, G.X. Zhang, X.Y. Shi, Targeted cancer theranostics using alpha-tocopheryl succinate-conjugated multi-functional dendrimer-entrapped gold nanoparticles, *Biomaterials* 35 (26) (2014) 7635–7646.
- [38] P.K. Maiti, T. Cagin, S.T. Lin, W.A. Goddard, Effect of solvent and pH on the structure of PAMAM dendrimers, *Macromolecules* 38 (3) (2005) 979–991.
- [39] J. Wang, D. Li, Y. Fan, M. Shi, Y. Yang, L. Wang, Y. Peng, M. Shen, X. Shi, Core-shell tecto dendrimers formed via host-guest supramolecular assembly as pH-responsive intelligent carriers for enhanced anticancer drug delivery, *Nanoscale* 11 (46) (2019) 22343–22350.
- [40] A. Sachdev, I. Matai, P. Gopinath, Dual-functional carbon dots-silver@zinc oxide nanocomposite: in vitro evaluation of cellular uptake and induction of apoptosis, *J. Mater. Chem. B* 3 (7) (2015) 1208–1220.
- [41] Y. Wang, X. Cao, R. Guo, M. Shen, M. Zhang, M. Zhu, X. Shi, Targeted delivery of doxorubicin into cancer cells using a folic acid-dendrimer conjugate, *Polym. Chem.* 2 (8) (2011) 1754–1760.
- [42] T.-G. Iversen, T. Skotland, K. Sandvig, Endocytosis and intracellular transport of nanoparticles: present knowledge and need for future studies, *Nano Today* 6 (2) (2011) 176–185.
- [43] W. Cheng, C. Liang, L. Xu, G. Liu, N. Gao, W. Tao, L. Luo, Y. Zuo, X. Wang, X. Zhang, X. Zeng, L. Mei, TPGS-functionalized polydopamine-modified mesoporous silica as drug nanocarriers for enhanced lung cancer chemotherapy against multidrug resistance, *Small* 13 (29) (2017) 1700623.
- [44] J. Zhu, F. Fu, Z. Xiong, M. Shen, X. Shi, Dendrimer-entrapped gold nanoparticles modified with RGD peptide and alpha-tocopheryl succinate enable targeted theranostics of cancer cells, *Colloids Surf., B* 133 (2015) 36–42.
- [45] F. Wang, Y.-C. Wang, S. Dou, M.-H. Xiong, T.-M. Sun, J. Wang, Doxorubicin-tethered responsive gold nanoparticles facilitate intracellular drug delivery for overcoming multidrug resistance in cancer cells, *ACS Nano* 5 (5) (2011) 3679–3692.
- [46] D. Sobot, S. Mura, P. Couvreur, How can nanomedicines overcome cellular-based anticancer drug resistance? *J. Mater. Chem. B* 4 (30) (2016) 5078–5100.
- [47] J. Xie, Y. Yong, X. Dong, J. Du, Z. Guo, L. Gong, S. Zhu, G. Tian, S. Yu, Z. Gu, Y. Zhao, Therapeutic nanoparticles based on curcumin and bamboo charcoal nanoparticles for chemo-photothermal synergistic treatment of cancer and radio-protection of normal cells, *ACS Appl. Mater. Interfaces* 9 (16) (2017) 14281–14291.
- [48] E.-M. Collnot, C. Baldes, U.F. Schaefer, K.J. Edgar, M.F. Wempe, C.-M. Lehr, Vitamin E TPGS P-glycoprotein inhibition mechanism: influence on conformational flexibility, intracellular ATP levels, and role of time and site of access, *Mol. Pharmaceutics* 7 (3) (2010) 642–651.
- [49] H. Mizutani, S. Tada-Oikawa, Y. Hiraku, M. Kojima, S. Kawanishi, Mechanism of apoptosis induced by doxorubicin through the generation of hydrogen peroxide, *Life Sci.* 76 (13) (2005) 1439–1453.
- [50] Z. Su, M. Chen, Y. Xiao, M. Sun, L. Zong, S. Asghar, M. Dong, H. Li, Q. Ping, C. Zhang, ROS-triggered and regenerating anticancer nanosystem: an effective strategy to subdue tumor's multidrug resistance, *J. Contr. Release* 196 (2014) 370–383.

- [51] X. Qu, F. Bian, Q. Guo, Q. Ge, Q. Sun, X. Huang, Ligation-rolling circle amplification on quantum dot-encoded microbeads for detection of multiplex G-quadruplex-forming sequences, *Anal. Chem.* 90 (20) (2018) 12051–12058.
- [52] Y. Zhuang, L. Zhao, L. Zheng, Y. Hu, L. Ding, X. Li, C. Liu, J. Zhao, X. Shi, R. Guo, LAPONITE-polyethylenimine based theranostic nanoplatform for tumor-targeting CT imaging and chemotherapy, *ACS Biomater. Sci. Eng.* 3 (3) (2017) 431–442.
- [53] B.D.M. Meijering, L.J.M. Juffermans, A. van Wamel, R.H. Henning, I.S. Zuhorn, M. Emmer, A.M.G. Versteilen, W.J. Paulus, W.H. van Gilst, K. Kooiman, N. de Jong, R.J.P. Musters, L.E. Deelman, O. Kamp, Ultrasound and microbubble-targeted delivery of macromolecules is regulated by induction of endocytosis and pore formation, *Circ. Res.* 104 (5) (2009) 679–687.
- [54] K. Ektate, A. Kapoor, D. Maples, A. Tuysuzoglu, J. VanOsdol, S. Ramasami, A. Ranjan, Motion compensated ultrasound imaging allows thermometry and image guided drug delivery monitoring from echogenic liposomes, *Theranostics* 6 (11) (2016) 1963–1974.